ACS APPLIED MATERIALS & INTERFACES

www.acsami.org

Research Article

Photoinduced Electron Transfer-Based Glutathione-Sensing Theranostic Nanoprodrug with Self-Tracking and Real-Time Drug Release Monitoring for Cancer Treatment

Safiya Nisar, Elisabeth Starosta, Mouhmad Elayyan, Amrit Regmi, and Binglin Sui*

Cite This: *ACS Appl. Mater. Interfaces* 2024, 16, 6859–6867

Read Online

ACCESS | Metrics & More | Article Recommendations | Supporting Information

ABSTRACT: The rapid development of nanomedicine has considerably advanced precision therapy for cancer treatment. Superior to traditional chemotherapy, emerging theranostic nanoprodrugs can effectively realize inherent self-tracking, targeted drug delivery, stimuli-triggered drug release, and reduced systemic toxicity of chemotherapeutic drugs. However, theranostic nanoprodrugs with real-time drug release monitoring have remained rare so far. In this work, we developed a new glutathione-responsive theranostic nanoprodrug with a high drug-loading content of 59.4 wt % and an average nanoscale size of 46 nm, consisting of the anticancer drug paclitaxel and a fluorescent imaging probe with a high fluorescence quantum yield, which are linked by a disulfide-based glutathione-sensitive self-immolating linker. The strong fluorescence emission of the fluorophore enables efficacious self-tracking and sensitive fluorescence "ON-OFF" glutathione sensing. Upon encountering high-level glutathione in cancer cells, the disulfide bond is cleaved, and the resulting linker halves spontaneously collapse into cyclic small molecules at the same pace, leading to the simultaneous release of the therapeutic drug and the fluorescence-OFF imaging probe. Thereby, the drug release process is efficiently monitored by the fluorescence change in the nanoprodrug. The nanoprodrugs exerted high cytotoxicity toward various cancer cells, especially for A549 and HEK-293 cells, in which the nanoprodrugs generated better therapeutic effects than free paclitaxel. Our work demonstrated a new modality of smart theranostic nanoprodrugs for precise cancer therapy.

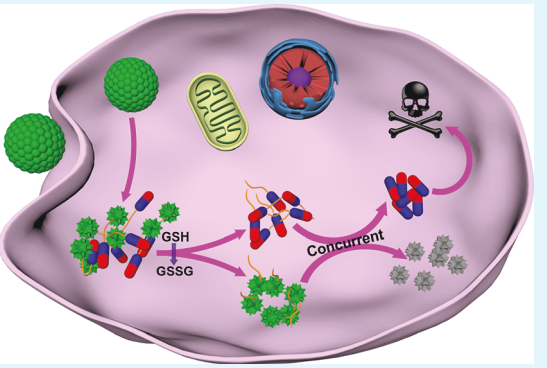

KEYWORDS: *theranostic nanomaterials, nanoprodrug, glutathione sensing, photoinduced electron transfer, self-tracking, real-time drug release monitoring, cancer therapy*

INTRODUCTION

Theranostic prodrugs are a class of medical agents that combine therapy and diagnosis functions into a single molecule, often composed of a therapeutic drug and a diagnostic probe.[1] The prodrug concept generally refers to a masked and inactive form of a drug produced by reversible modification of the parent drug, which is equipped with more desirable physicochemical properties and is ready to be converted back to the bioactive drug in the body.[2−6] Nanoparticulate prodrugs, or nanoprodrugs (NPDs), have been proven even more efficient in accumulating at tumor sites due to the enhanced permeability and retention (EPR) effect.[7−9] By including an imaging moiety within an NPD, it becomes possible to track its distribution, metabolism, and therapeutic response in real time, ultimately leading to precise cancer chemotherapy.

Traditional theranostic prodrugs/NPDs are generally produced via linking an imaging agent (e.g., a fluorescent dye) and a drug molecule by a biocleavable linker. Such theranostics are capable of self-tracking due to the fluorescence emission but cannot indicate drug release because of the lack of changes in the fluorescence signals. Recent developments in the field brought alternative counterparts that can reflect the drug release by emitting fluorescence. They switch from a nonfluorescent state to a fluorescent one, the so-called fluorescence "OFF-ON" process, in response to external stimuli. However, self-tracking is not allowed with these theranostics due to their nonfluorescent nature. Also, they are unsuitable for real-time drug release monitoring because the fluorescence emission may become saturated and, thus, lose sensitivity as more bioactive drug molecules are released. Therefore, fluorescent NPDs that can turn off the fluorescence emission responding to certain stimuli, the fluorescence "ON-OFF" mechanism, would be advantageous for attaining both

Received: November 6, 2023
Revised: December 26, 2023
Accepted: January 19, 2024
Published: February 1, 2024

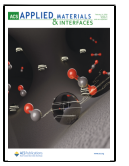

self-tracking and drug release signaling. Furthermore, it would be even superior if the drug release process could be monitored in real time, by which the metabolism of NPDs and the complete release of bioactive drug molecules could be determined efficiently. To the best of our knowledge, theranostic prodrugs/NPDs capable of real-time monitoring of the drug release are seldom.

Photoinduced electron transfer (PeT), a chemical process in which an electron is transferred from one functional group to another upon absorption of light, is of crucial importance in a wide range of chemical processes, including photochemical reactions, photoredox catalysis, photovoltaics, and fluorescent sensors.[10−13] The high signal-to-noise ratios of PeT-based fluorescent probes render them desired for imaging various species in biological environments.[13] As known, cancer cells overexpress a large amount of glutathione (GSH) for the purpose of drug resistance compared with normal cells, and thus, the levels of GSH in tumor tissues (2−10 mM) are abnormally higher than those in the bloodstream and healthy tissues (2−20 μM).[14,15] Due to the importance of GSH in cancer treatment, a myriad of GSH-involved fluorescent probes and drug delivery systems have been reported over the past two decades.[16−23] However, PeT-based theranostic NPDs that can simultaneously sense GSH and release therapeutic drug molecules in the tumor microenvironment have remained rare.

Herein, we intend to develop a GSH-sensitive self-tracking theranostic NPD that can temporally monitor the drug release in cells by incorporating a highly photostable fluorescent probe with a high fluorescence quantum yield and anticancer therapeutic drug paclitaxel (PTX) linked by a symmetric disulfide-containing self-immolating linker. As depicted in Figure 1, the strong fluorescence emission and high photostability of the imaging moiety will make it convenient to track the self-delivering NPD and record the fluorescence changes. Upon entering cancer cells, the disulfide bond of NPDs is cleaved by the high-level intracellular GSH of cancer cells. Subsequently, the cleaved linker will self-immolate into nontoxic small molecules, concurrently turning off the strong fluorescence signals and releasing PTX molecules in a traceless manner, achieving the desired cancer chemotherapy while monitoring real-time drug release.

RESULTS AND DISCUSSION

Hypothesis and Molecule Design. Boron-dipyrromethene (BODIPY, Figure 2) dyes have been broadly explored for bioimaging applications owing to their desirable photophysical properties, including high quantum yields, excellent photostability, zero net charge, biocompatibility, and sharp absorption and emission peaks.[24−27] A variety of amino groups have been attached to BODIPY derivatives to construct PeT-based fluorescent sensors for biological targets, in which the amino group serves as the electron donor, donating one of the lone-pair electrons of the nitrogen atom, and the BODIPY core as the electron acceptor.[28−36] Based on the PeT theory, we hypothesized that the BODIPY-amino conjugate (BDP-A1), as shown in Figure 2, would emit weak fluorescence due to the PeT effect; and compound BDP-B1, in which an electron-withdrawing *tert*-butyloxycarbonyl (Boc) group is bonded to the amino group and thus reduces the activity of the lone pair of the nitrogen atom, would emit strong fluorescence because the lone-pair electrons are no longer available for the PeT effect.

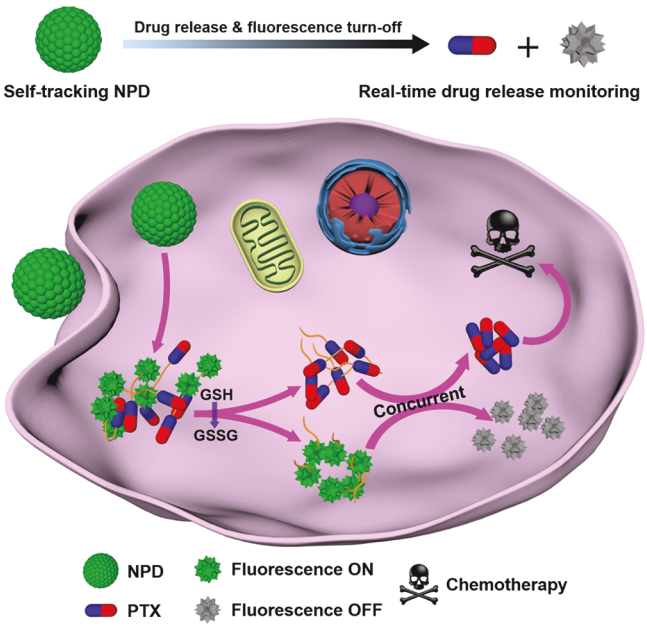

Figure 1. Schematic illustration of the PTX NPD achieving self-tracking, intracellular real-time drug release monitoring, and cancer chemotherapy. The fluorescence-emitting NPDs can be converted into fluorescence-OFF dye molecules and free PTX with their intact chemical structure and therapeutic effect. Once entering cancer cells, the self-tracking NPDs are disassembled and the liberated fluorescence-ON theranostic prodrugs are cleaved by the high-level intracellular GSH, which subsequently leads to the concurrent fluorescence turn-off of the dye and release of PTX molecules, attaining real-time monitoring of drug release and cancer therapy.

Theoretical Modeling. In order to validate our hypothesis, we calculated the frontier molecular orbitals of PeT-involved moieties in BDP-A1 and BDP-B1 using density functional theory (DFT) calculations at the CAM-B3LYP level. As shown in Figure 3, the highest occupied molecular orbital (HOMO) energy of the BODIPY moiety at the excited state was calculated to be −6.741 eV, which is lower than that of the amino group (−6.384 eV), allowing for electron transfer from the amino group to the BODIPY moiety. As a result, the fluorescence of BODIPY will be quenched by the amino group. However, the HOMO energy of the −NH-Boc unit (−6.784 eV) is lower than that of the BODIPY moiety, indicating that there is no electron transfer from the −NH-Boc unit to the BODIPY moiety, and thus, the PeT process is prohibited. These calculations verified the hypothesis that BDP-B1 will be highly fluorescent while BDP-A1 will emit negligible fluorescence due to the PeT effect.

Synthesis and Characterization. To experimentally confirm our hypothesis, BDP-A1 and BDP-B1 were synthesized via Sonogashira coupling reactions (Scheme S1) according to previously reported synthetic methods.[37−39] Their chemical structures were characterized by nuclear magnetic resonance (NMR) spectroscopy and high-resolution mass spectrometry (HRMS). Besides, BDP-A2 and BDP-B2 (Figure 2), in which the amino and Boc-bonded amino groups are attached to the BODIPY core from the vertical direction, respectively, were also synthesized, characterized, and investigated in the following experiments for comparison with BDP-A1 and BDP-B1 (Scheme S1).

Photophysical Properties. The absorption and emission properties of the synthesized BODIPY dyes were measured by

https://doi.org/10.1021/acsami.3c16585
ACS Appl. Mater. Interfaces 2024, 16, 6859−6867

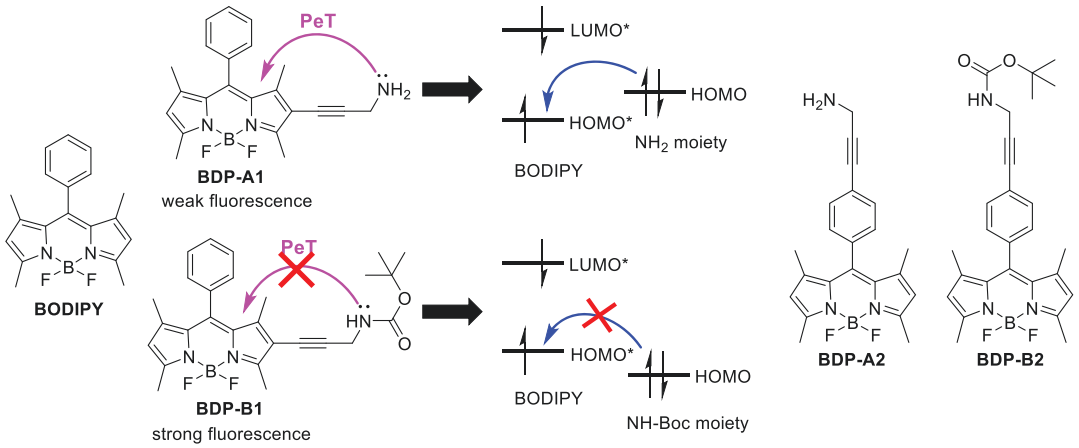

Figure 2. Chemical structures of BODIPY, BDP-A1, BDP-B1, BDP-A2, and BDP-B2, and the PeT-related HOMOs and lowest unoccupied molecular orbitals (LUMOs) (*excited state) of functional groups in BDP-A1 and BDP-B1.

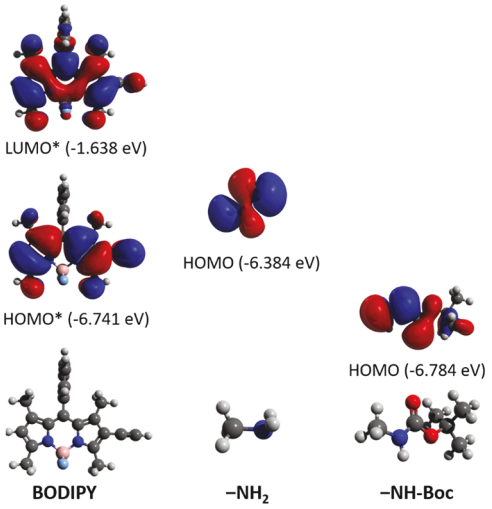

Figure 3. Frontier molecular orbital profiles of BODIPY (*excited state), $-NH_2$, and –NH-Boc based on the DFT calculation.

UV–vis and fluorescence spectroscopy, respectively. BDP-A1 showed an absorption peak at 501 nm and a fluorescence emission peak at 536 nm (Figure S1). As expected, BDP-A1 emitted very weak fluorescence with a fluorescence quantum yield (FLQY) of 0.05 (Table S1), whereas striking fluorescence was emitted by BDP-B1 (FLQY: 0.62). These results confirmed our hypothesis that an effective PeT effect exists in BDP-A1 from the amino donor to the excited BODIPY core but not in BDP-B1 (Figure 2).

On the other hand, BDP-A2 and BDP-B2 both displayed absorption wavelengths at 500 nm and fluorescence emission wavelengths at 511 nm (Figure S2). Different from BDP-A1, BDP-A2 emitted strong fluorescence (FLQY: 0.48), as strong as that of BDP-B2 (FLQY: 0.47) (Table S1), indicating the deficiency of the PeT effect in BDP-A2. Such a property can be ascribed to the non-π-conjugation between the *meso*-phenyl group and the BODIPY core, which are noncoplanar because of the steric effect caused by the methyl groups,[40] as depicted in Figure 3; thus, the PeT effect is disabled in BDP-A2 by the extended distance between the amino group and the BODIPY core.

BDP-A1 and BDP-A2 were further studied at varied pH values to evaluate their suitability for applications in biological environments. The fluorescence emission signals of BDP-A1 remained unchanged in solutions with pH values larger than 6.5 (Figure S3). However, as the pH decreased below 6.5, the fluorescence intensity of BDP-A1 gradually elevated. This phenomenon resulted from the protonation of the amino group, which deactivated the PeT effect in BDP-A1.[41−43] The observations demonstrated that BDP-A1 is not pH-dependent in physiological environments. In contrast, the fluorescence emission of BDP-A2 was barely affected by pH (Figure S4), which further corroborated the absence of PeT in this compound.

Toxicity and Cell Imaging. The toxicity of BDP-A1, BDP-B1, BDP-A2, and BDP-B2 was evaluated in cervical cancer HeLa cells by the 3-(4,5-dimethylthiazol-2-yl)-2,5-diphenyl tetrazolium bromide (MTT) assay at varying concentrations. None of the BODIPY derivatives induced considerable damage to cancer cells upon incubation at a concentration of 50 μM for 24 h (Figure S5), suggesting the low toxicity of the fluorescent probes. Cell imaging experiments were also conducted in HeLa cells by using confocal laser scanning microscopy (CLSM). Strong fluorescence was observed in cells incubated with BDP-B1, BDP-A2, and BDP-B2, whereas cells treated with BDP-A1 emitted very weak fluorescence (Figure S6), which aligned with their fluorescence emission properties (Table S1).

GSH Sensor Design. Based on the largely different performance of BDP-A1 and BDP-B1 in CLSM cell imaging, we designed a BDP-A1-derived fluorescent sensor (BDP-NPC, Figure 4A) for biological GSH detection. BDP-NPC was synthesized with BDP-A1 as the starting material (Scheme S2). Similar to BDP-B1, the amino group is masked into a carbamate group in BDP-NPC; therefore, the sensor is expected to be fluorescence-emitting. As known, the disulfide bond is sensitive to redox and can be cleaved by GSH to generate thiolate ions. Various disulfide-based GSH sensors and redox-responsive drug delivery systems have been reported in recent years.[44−46] Herein, a disulfide bond is linked to the carbamate group in BDP-NPC, serving as the GSH-sensing unit. As expected, BDP-NPC emitted strong fluorescence at 510 nm (Figure S7), and its FLQY was determined to be 0.67 (Table S1), resulting from the prohibited PeT effect.

GSH-Sensing Mechanism and Behaviors of BDP-NPC. Figure 4A shows the mechanism of the GSH-induced fluorescence "ON-OFF" process of BDP-NPC. In the presence

https://doi.org/10.1021/acsami.3c16585
ACS Appl. Mater. Interfaces 2024, 16, 6859−6867

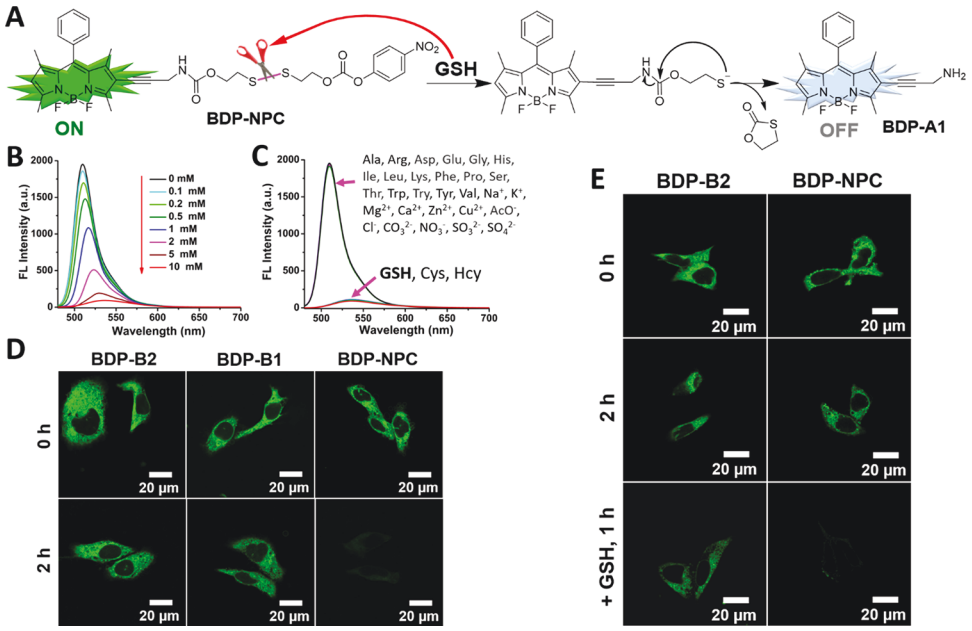

Figure 4. (A) GSH-sensing mechanism of BDP-NPC and the conversion to BDP-A1; fluorescence emission spectra of BDP-NPC (10 μM) upon addition of (B) GSH at varied concentrations (0−10 mM), and (C) various biologically related species, including GSH, Cys, Hcy, and other common amino acids at the concentration of 10 mM, and cations and anions at the concentration of 1.0 mM; (D) CLSM images of HeLa cells after incubation with BDP-B1, BDP-B2, and BDP-NPC for 30 min (0 h time point) and subsequent incubation in fresh medium for 2 h (2 h time point); and (E) CLSM images of NEM-pretreated HeLa cells after incubation with BDP-B2 and BDP-NPC for 30 min (0 h time point), subsequent incubation in fresh medium for 2 h (2 h time point), and then treatment with 10 mM GSH for 1 h (+ GSH, 1 h time point).

of GSH, the disulfide bonds of BDP-NPC molecules are cleaved, producing highly nucleophilic thiolate anions. The resulting thiolate ion intramolecularly attacks the electrophilic carbamate group, and consequently, the broken disulfide-carbamate linker self-immolates into a stable small molecule containing a five-member ring. At the same time, an amino group is regenerated, and BDP-NPC is converted back to BDP-A1, switching from fluorescence-ON to fluorescence-OFF.

To verify the mechanism, we measured the fluorescence response of BDP-NPC toward GSH at varied concentrations. As shown in Figure 4B, with increasing GSH concentration, the fluorescence intensity decreased accordingly, and meanwhile, the fluorescence emission maximum shifted gradually from 510 to 536 nm. After 10 mM GSH was added, a 21.3-fold decline in the fluorescence intensity was recorded. The limit of detection (LOD) was determined to be 0.21 μM according to the standard LOD calculation equation: LOD = $K \times \sigma/S$, where coefficient K = 3, σ is the standard derivation of the blank solution, and S is the slope of the calibration curve. Moreover, MS analysis showed that BDP-A1 molecules were detected in the resulting solution (Figure S8). The observed fluorescence "ON-OFF" and MS analysis results confirmed the plausibility of the GSH sensor design.

In addition, the fluorescence responses of BDP-NPC toward other biologically important species were investigated. As shown in Figure 4C, the addition of cysteine (Cys) and homocysteine (Hcy) also caused a fluorescence decrease comparable to that of GSH. However, they are not major thiol-containing species in cancer cells.[17] Given the low physiological levels of those compounds, the interfering effects will be negligible in cellular environments. Moreover, no significant fluorescence response was found in the presence of other species, including common amino acids (Ala, Arg, Asp, Glu, Gly, His, Ile, Leu, Lys, Phe, Pro, Ser, Thr, Trp, Try, Tyr, and Val), cations (Na^+, K^+, Mg^{2+}, Ca^{2+}, Zn^{2+}, and Cu^{2+}), and anions (AcO^-, Cl^-, CO_3^{2-}, NO_3^-, SO_3^{2-}, and SO_4^{2-}). Therefore, BDP-NPC has the potential to be exploited as a practical fluorescent probe for sensing GSH in cells.

Cellular GSH Sensing. The GSH sensing of BDP-NPC was further studied in cells. MTT assay tests showed that the probe induced minimal cytotoxicity to cells (Figure S9). Upon incubation with BDP-NPC, cells displayed strong fluorescence, indicating the existence of BDP-NPC in cells (Figure S10). To examine its response to intracellular GSH, cells were cultured in a fresh medium for 2 h, following incubation with BDP-NPC for 30 min. As shown in Figure 4D, strong fluorescence was observed in cells right after the incubation (0 h time point). After 2 h in the fresh medium, the fluorescence became very weak (2 h time point), reflecting that cleavage of the disulfide bond of BDP-NPC led to the generation of nonfluorescent BDP-A1 (Figure 4A). On the contrary, cells incubated with BDP-B1 and BDP-B2 constantly emitted fluorescence during the same time interval. To further evidence that the fluorescence decrease resulted from GSH-triggered disulfide cleavage, cells were pretreated with N-ethylmaleimide (NEM), which reacts with GSH to yield a stable compound GS-NEM and thus is widely used as a GSH-blocking agent,[47,48] for 1 h before incubation with BDP-NPC. As a result, strong fluorescence was still emitted by cells after incubation in the fresh medium for 2 h, as shown in Figure 4E, which implied that BDP-NPC stayed intact in the absence of intracellular GSH. Further treatment with 10 mM GSH substantially diminished the fluorescence emission of cells. In contrast, cells incubated with BDP-B1 remained fluorescent throughout the same treatments. All of the results suggest that BDP-NPC can respond to GSH and be converted to BDP-A1 in live cells.

https://doi.org/10.1021/acsami.3c16585
ACS Appl. Mater. Interfaces 2024, 16, 6859−6867

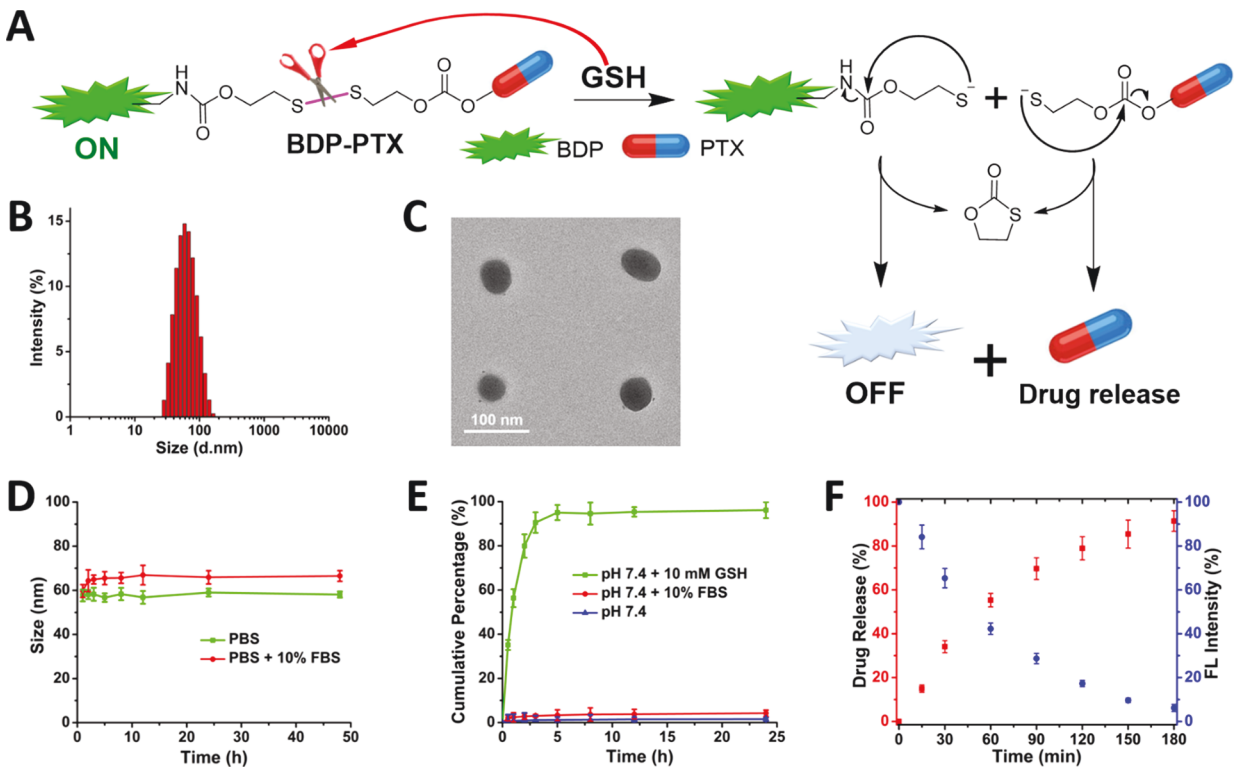

Figure 5. (A) GSH-triggered simultaneous release of BDP-A1 and free PTX from BDP-PTX. (B) Size distribution and (C) TEM image of BDP-PTX NPD. (D) Size changes of the NPDs in PBS (pH 7.4) and PBS + 10% FBS solutions. (E) Drug release profiles of BDP-PTX NPD in PBS (pH 7.4), PBS + 10% FBS, and PBS + 10 mM GSH solutions. (F) Time-lapsed concurrent drug release and fluorescence intensity decrease of BDP-PTX NPD upon incubation with 10 mM GSH. Data represent the means ± SD, $n = 3$.

GSH-Responsive Theranostic Prodrug Design. On the basis of the PeT-based GSH sensor, we designed a theranostic prodrug (BDP-PTX) consisting of a BODIPY fluorophore, anticancer drug PTX, and a GSH-responsive linker (Figure 5A). In the prodrug design, the PTX moiety is bonded to the GSH-sensitive linker via a carbonate group, which is analogous to a carbamate group and is also electrophilic and vulnerable to attack by a thiolate ion. The same as the thiolate-carbamate linker, the thiolate-carbonate linker self-immolates as well, turning into the same small molecule and releasing PTX as a free drug, as illustrated in Figure 5A. Consequently, the cleavage of disulfide bonds will lead to the concurrent self-immolation of the two broken halves, simultaneously releasing BDP-A1 and free PTX molecules. Therefore, it is highly promising to achieve real-time monitoring of the drug release of BDP-PTX by recording the changes in its fluorescence emission.

Theranostic NPD Formulation. The synthesis of BDP-PTX is straightforward and completed in one step, beginning with the BDP-NPC (Scheme S3). It exhibits fluorescence emission at 511 nm (Figure S11), and its photophysical properties are comparable to those of BDP-NPC (Table S1) due to the similarity in their chemical structures. As expected, BDP-PTX is equivalent to BDP-NPC in responding to GSH and other biological species (Figure S12). Besides, we found that the prodrug BDP-PTX could be assembled into a nanostructure, BDP-PTX NPD, upon dispersion into aqueous media, attributed to the intermolecular $\pi-\pi$ stacking and hydrophobic interaction.[49,50] The NPDs were characterized by dynamic light scattering (DLS) and transmission electron microscopy (TEM). DLS data indicated that BDP-PTX NPD had an average hydrodynamic size of 58.6 nm with a narrow distribution (PDI = 0.132; Figure 5B) and a negative surface charge of −18.5 mV. TEM imaging observed a spherical-shaped morphology and a size of about 46 nm for the NPDs (Figure 5C). As a carrier-free drug delivery nanosystem, BDP-PTX NPD showed an excellent drug-loading content (59.4%, w/w), much higher than that of traditional PTX-delivering systems (typically 10−15%). Moreover, the NPDs exhibited desirable colloidal stability, as evidenced by the barely changed hydrodynamic size in water for 1 week (Figure S13). The high stability was also observed in a phosphate-buffered solution (PBS, pH 7.4) with and without fetal bovine serum (FBS). As shown in Figure 5D, the size of BDP-PTX NPD enlarged by ∼12% within the first 2 h upon dispersion into a PBS solution containing 10% FBS, which might result from protein adsorption on the surface, and thereafter, the average hydrodynamic diameter remained stable in the next 46 h. Furthermore, the NPDs turned off the fluorescence emission in response to the presence of GSH (Figure S14).

Fluorescence-Signaled Drug Release. Efficient drug release is an indispensable property for a practical prodrug/NPD, as the masked bioactive drug molecules must be released from the drug-delivering systems to execute the desired therapeutic effects. We studied the PTX release profile of BDP-PTX NPD in various release media mimicking diverse biological environments. As shown in Figure 5E, in PBS buffer (pH 7.4) with and without 10% FBS, no considerable amount of PTX was released from the NPDs. However, in the presence of 10 mM GSH in PBS buffer (pH 7.4), a quick release of PTX was observed, and the cumulative percentage of released PTX attained ∼90% within 3 h of incubation and >95% in 24 h. MS

https://doi.org/10.1021/acsami.3c16585
ACS Appl. Mater. Interfaces 2024, 16, 6859−6867

analysis of the ingredients in the release media confirmed the release of free PTX molecules as well as BDP-A1 (Figure S15). Similar to the fluorescence response of BDP-NPC to GSH (Figure 4B), the drug release efficiency of the NPDs was also affected by the concentration of GSH, with lower GSH levels leading to slower drug release (Figure S16). Furthermore, the cumulative drug release increased while the fluorescence intensity of the NPDs decreased gradually, as shown in Figure 5F, and more interestingly, the drug release and the fluorescence decrease of BDP-PTX NPD occurred at the same pace, which indicates the promise of this NPD to achieve real-time monitoring of drug release in cells.

Real-Time Monitoring of Intracellular Drug Release. CLSM imaging showed that BDP-PTX NPDs could effectively enter the cells (Figure S17). As a fluorescent prodrug derived from BDP-NPC, BDP-PTX exhibited fluorescence "ON-OFF" in cells, as well. Figure 6A shows the time-lapsed fluorescence images of HeLa cells taken at different postincubation time points (0, 30, 60, 90, and 120 min). Cells emitted strong fluorescence upon incubation with BDP-PTX NPDs for 30 min (0 min time point). During the following incubation in the fresh medium, the fluorescence of cells became weaker and basically disappeared after 2 h (120 min time point). In contrast, cells incubated with the reference dye BDP-B2 displayed a slight decrease in fluorescence emission after the same treatments. The average fluorescence intensity of cells versus time was plotted in Figure 6B, which quantitatively demonstrated the decline in cell fluorescence. Meanwhile, in addition to the CLSM imaging, cells were lysed at each postincubation time point, and the drug contents in the cell lysates were determined to reveal the temporal intracellular drug release. As shown in Figure 6C, the percentage of released free PTX kept increasing during the 120 min postincubation, which is in good agreement with the fluorescence decrease of cells (Figure 6B). Thereby, the drug release of BDP-PTX NPD in cells is temporally reflected by the fluorescence intensity change of cells, attaining noninvasive real-time intracellular drug release monitoring.

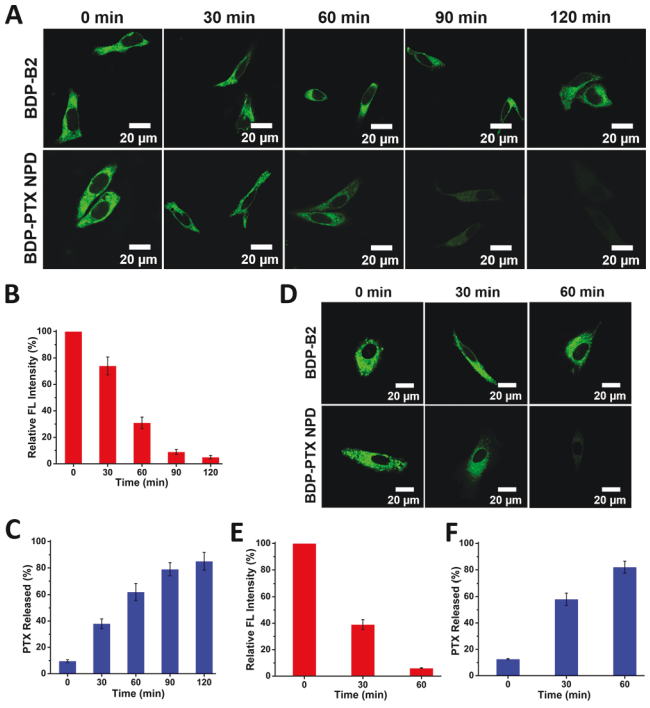

Figure 6. (A) CLSM images of HeLa cells, (B) relative fluorescence intensity, and (C) percentage of PTX released in cells after incubation with BDP-PTX NPD for 0, 30, 60, 90, and 120 min. (D) CLSM images of A549 cells, (E) relative fluorescence intensity, and (F) percentage of PTX released in cells after incubation with BDP-PTX NPD for 0, 30, and 60 min. Data represent the means ± SD, n = 3.

To further validate the effectiveness of BDP-PTX NPD in indicating real-time intracellular drug release, we conducted the same experiments in A549 cancer cells. Interestingly, fluorescence turn-off was even faster than that in HeLa cells. As shown in Figure 6D, the fluorescence emission of cells decreased drastically and almost disappeared within 1 h. The concurrent decrease in fluorescence intensity and increase in drug release consolidated the drug release monitoring ability of the NPD (Figure 6E,F). Additionally, pretreatment with NEM effectively inhibited the fast fluorescence change and drug release in cells (Figure S18). The quicker responses in fluorescence emission and drug release of BDP-PTX NPD might result from the high intracellular levels of GSH in A549 cells (8.3 mM), compared to those in HeLa cells (4.4 mM).[17] These results further verified the high efficiency of BDP-PTX NPD in monitoring real-time drug release in cells.

In Vitro Anticancer Efficacy. The therapeutic effects of BDP-PTX NPD against cancer were first evaluated in HeLa cells by the MTT assay. Figure 7A shows the viability of cells upon incubation with free PTX and NPDs at equivalent PTX concentrations for 24 h. Both of them exerted inhibitory effects on cell growth in a dose-dependent fashion. To achieve better therapeutic outcomes, we extended the incubation time to 72 h, and as a result, the cell growth was substantially suppressed by both treatments (Figure 7B). BDP-PTX NPD exhibited comparable anticancer efficacy as free PTX at higher doses. In addition, the antiproliferation ability of the NPDs was further

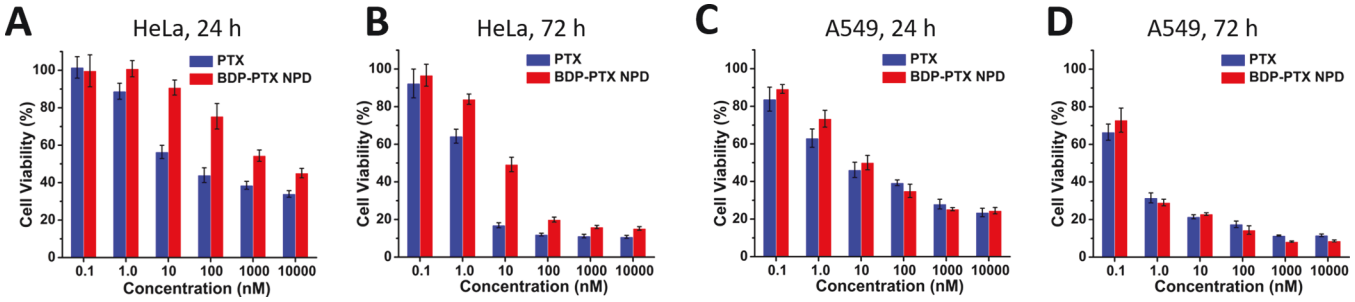

Figure 7. Cell viability of cancer cells after incubation with free PTX and BDP-PTX NPD: (A) HeLa cells for 24 h, (B) HeLa cells for 72 h, (C) A549 cells for 24 h, and (D) A549 cells for 72 h. Data represent the means ± SD, n = 3.

https://doi.org/10.1021/acsami.3c16585
ACS Appl. Mater. Interfaces 2024, 16, 6859−6867

evaluated in other cancer cells, including A549 (Figure 7C,D), DU145 (Figures S19A and S20A), HCT116 (Figures S19B and S20B), HEK-293 (Figures S19C and S20C), HT-29 (Figures S19D and S20D), HT-1080 (Figures S19E and S20E), MCF7 (Figures S19F and S20F), MDA-MB-231 (Figures S19G and S20G), MDA-MB-468 (Figures S19H and S20H), MIA PaCa-2 (Figures S19I and S20I), PANC-1 (Figures S19J and S20J), and SW480 (Figures S19K and S20K). The proliferation of all the cells was inhibited by the NPDs to varied extents. It is noteworthy that BDP-PTX NPD imposed higher suppression toward the proliferation of A549 cells (Figure 7D) and HEK-293 cells (Figure S20C) than free PTX after incubation for 72 h. The higher cancer inhibition effect may result from higher levels of intracellular GSH in those cells. The results confirmed the effectiveness of the theranostic NPD strategy in cancer treatment and its potential for developing precise chemotherapy with real-time drug monitoring.

CONCLUSIONS

A self-tracking GSH-sensing theranostic NPD (BDP-PTX NPD) has been developed to realize real-time drug release monitoring for precise cancer treatment. In the prodrug molecules, the anticancer drug PTX and a fluorescent probe with a high fluorescence quantum yield are bridged by a symmetric GSH-sensitive self-immolating linker. The imaging moiety exhibits fluorescence "ON-OFF" behaviors as a response to GSH but not to other physiologically related species. Upon encountering GSH, the biocleavable linker is cleaved and subsequently self-immolates into stable cyclic molecules, simultaneously turning off its fluorescence emission and releasing bioactive PTX molecules. Due to the same pace of the two processes, the drug release is efficiently reflected by the fluorescence response in real time. Based on the advantages, we have successfully monitored the real-time drug release of BDP-PTX NPD in cancer cells. Meanwhile, NPD has demonstrated desired therapeutic effects toward the proliferation of cancer cells. A limitation of the NPD is that its fluorescence emission wavelength is located in the visible light region, which hinders its real-time drug release monitoring in vivo. The development of a new self-tracking theranostic NPD bearing an imaging unit with near-IR fluorescence emission is ongoing in our laboratory. Overall, our research has provided a strategy to develop theranostic NPDs with self-tracking and real-time drug release monitoring for precise chemotherapy.

MATERIALS AND METHODS

Materials. Benzaldehyde, 4-iodobenzaldehyde, 2,4-dimethylpyrrole, trifluoroacetic acid (TFA), triethylamine (TEA), N-(tert-butoxycarbonyl)propargylamine, 2,3-dichloro-5,6-dicyano-1,4-benzoquinone (DDQ), boron trifluoride diethyl ether complex (BTF), CuI, Tetrakis(triphenylphosphine)palladium(0) [$Pd(PPh_3)_4$], N-iodosuccinimide (NIS), 4-nitrophenyl chloroformate, 2-hydroxyethyl disulfide, L-glutathione (GSH), PBS, DL-dithiothreitol (DTT), paraformaldehyde (PFA), (3-(4,5-dimethylthiazol-2-yl)-2,5-diphenyltetrazolium bromide (MTT), and silica gel (spherical, 100 μm) were purchased from Thermo Fisher Scientific, Inc. (Waltham, MA, USA). Paclitaxel (PTX) was purchased from LC Laboratories (Woburn, MA, USA). Cremophor EL was purchased from EMD Millipore Corp. (Billerica, MA, USA). Gibco Dulbecco's modified Eagle's medium (DMEM), FBS, penicillin-streptomycin (PS), trypsin-EDTA, and Invitrogen Hoechst 33342 were purchased from Thermo Fisher Scientific, Inc. (Waltham, MA, USA). Deuterated chloroform and dimethyl sulfoxide solvents were purchased from Cambridge Isotope Laboratories, Inc. (Andover, MA, USA). All of the other solvents used in this research were purchased from Thermo Fisher Scientific, Inc. (Waltham, MA, USA) and directly used without further purification.

Photophysical Properties. Spectroscopic properties of all materials were measured in 10 mm path length quartz cuvettes at room temperature. UV−vis absorption was measured with a PerkinElmer Lambda 1050 UV/vis/NIR spectrophotometer. Fluorescence emission spectra were obtained by using a Shimadzu RF-6000 spectrophotometer. All the measurements were conducted with an optical density no higher than 0.12 at excitation wavelength to avoid reabsorption. Fluorescence quantum yields were calculated by a standard relative method using the equation below with Rhodamine 6G ($\Phi_{FL} \approx 0.94$ in ethanol) as a reference:

$$\Phi_{FL} = \Phi_R \frac{I}{I_R} \frac{OD_R}{OD} \frac{n^2}{n_R^2} \frac{RP_R}{RP}$$

where Φ is the quantum yield, subscript R refers to the reference, I is the integrated emission signal, OD is the optical density at the excitation wavelength, n is the refractive index of the solvent, and RP is the relative power of the light source of the spectrofluorometer at the excitation wavelength.

GSH-Sensing Experiments. Stock solutions of GSH, Hcy, Cys, amino acids (Ala, Arg, Asp, Glu, Gly, His, Ile, Leu, Lys, Phe, Pro, Ser, Thr, Trp, Try, Tyr, and Val), cations (Na^+, K^+, Mg^{2+}, Ca^{2+}, Zn^{2+}, and Cu^{2+}), and anions (AcO^-, Cl^-, CO_3^{2-}, NO_3^-, SO_3^{2-}, and SO_4^{2-}) were prepared in DI water at the concentration of 0.1 M. Stock solutions of BDP-NPC and BDP-PTX with the concentration of 10 mM were prepared in acetonitrile and diluted with PBS buffer (pH 7.4). The UV−vis absorption and fluorescence emission spectra were measured in PBS solution (pH 7.4) with 20% (v/v) acetonitrile. All samples were incubated in the dark at 37 °C for 3 h prior to measurements.

Formulation of the NPD. BDP-PTX NPD was prepared via a nanoassembling procedure. The BDP-PTX prodrug was dissolved in acetone and then dispersed into DI water under vigorous stirring. The prodrug molecules were assembled into nanostructures spontaneously. Acetone in the resulting mixture was evaporated under reduced pressure at room temperature. The final NPD was stored at 4 °C for future use. The particle size, polydispersity index (PDI), and surface charge of the NPDs were measured by DLS using a Zetasizer (Nano ZS, Malvern Instruments Ltd., Malvern, UK). The morphology of BDP-PTX NPD was imaged by a Hitachi HT7500 TEM (Hitachi High-Technologies Corporation, Tokyo, Japan). The amount of PTX contained in the NPDs was determined by HPLC, and the drug-loading content was calculated by the following equation:

$$\text{Drug content (\%)} = \frac{\text{weight of the drug in NPDs}}{\text{weight of the NPDs}} \times 100\%$$

Colloidal Stability. The colloidal stability of the NPDs was obtained by DLS analysis. NPDs were first dispersed into PBS buffer (pH 7.4) and PBS buffer with 10% FBS (pH 7.4) and then incubated at 37 °C. The hydrodynamic size of the NPDs was determined with DLS at predetermined time points.

Fluorescence-Signaled Drug Release. The release profiles of PTX from BDP-PTX NPD were recorded at 37 °C with PBS buffer solutions (pH 7.4) containing 20% (v/v) acetonitrile as the release media. The NPDs (equivalent to 200 nmol of PTX) were incubated in the release media with and without 10% FBS or 10 mM GSH in the dark. At predetermined time points, 1 mL of the release medium was sampled and diluted with acetonitrile. The concentrations of released PTX were immediately analyzed by high-performance liquid chromatography (HPLC), and the fluorescence emission spectra were recorded on the spectrophotometer. The ingredients in the final release media were measured by high-resolution mass spectrometry (HRMS).

Cell Culture. Human cancer cells HeLa, A549, DU145, HCT116, HEK-293, HT-29, HT-1080, MCF7, MDA-MB-231, MDA-MB-468, MIA PaCa-2, PANC-1, and SW480 were cultured in Dulbecco's

https://doi.org/10.1021/acsami.3c16585
ACS Appl. Mater. Interfaces 2024, 16, 6859−6867

Modified Eagle's Medium (DMEM, Gibco) supplemented with 10% FBS, 100 units/mL penicillin, and 100 μg/mL streptomycin. All cells were cultured at 37 °C in 100 mm culture dishes under a humidified atmosphere of 5% CO_2. Cells were subcultured when the cell confluence reached 70−80%.

Confocal Fluorescence Imaging and Real-Time Drug Release Monitoring. Fluorescence images of cells were recorded by CLSM. Cells were seeded at a density of 200,000 cells/dish in a 35 mm^2 Petri dish with a glass window at the bottom for 24 h at 37 °C with 5% CO_2 . After washing with PBS (pH 7.4), cells were incubated with BDP probes or the NPD for 3 h. Cells cultured in fresh medium without any incubation were used as a control. All cells were washed with PBS three times and fixed with paraformaldehyde (4% in PBS) for 10 min at room temperature. Following the removal of paraformaldehyde, cells were further washed with PBS three times, and the nuclei of cells were stained with Hoechst 33342 (final concentration 1 μg/mL) for 10 min. After three more washings with PBS, cells were imaged under a confocal microscope (Olympus FV3000 Laser Scanning Confocal Microscope).

For GSH-blocking tests, cells were incubated with 10 mM N-ethyl maleimide (NEM) in an FBS-free medium for 1 h at 37 °C. The remaining NEM was removed, and cells were washed with PBS buffer three times. Cells were further treated with fresh medium containing 20 μM BDP-NPC or BDP-PTX NPD for 30 min. After being washed with PBS buffer, cells were imaged by confocal microscopy. Cells were incubated in fresh medium for 2 h and imaged by confocal microscopy. Then, cells were treated with fresh medium containing 10 mM GSH for 1 h and imaged by confocal microscopy.

For monitoring real-time drug release, cells were incubated with fresh medium containing 20 μM BDP-PTX NPD for 30 min. After being washed with PBS buffer, cells were incubated in fresh medium. Then, cells were imaged at predetermined time points by confocal microscopy. Meanwhile, at the same time points, the culture medium was removed and the cells were treated with RIPA lysis buffer. The cell lysate mixture was gently shaken for 15 min at room temperature. The resulting cell lysates combined with the cell culture medium were extracted with dichloromethane three times. The collected extract was analyzed by HPLC to determine the percentage of released PTX in the drug/prodrug mixture.

Cytotoxicity Assay. The toxicity of fluorescent probes and the therapeutic effects of BDP-PTX NPD against cancer cells was evaluated by 3-(4,5-dimethylthiazole-2-yl)-2,5-diphenyltetrazolium ammonium bromide (MTT) assay. Cells were seeded at a density of 5,000 cells/well in 96-well plates at 37 °C with 5% CO_2 for 24 h before the test. In the tests, cells were incubated with fresh medium containing those probes, free PTX, or the NPD at varied concentrations for 24 or 72 h. In the control group, cells were cultured in a fresh medium without any treatment. Thereafter, the medium was replaced with a solution of the MTT reagent in fresh medium at a concentration of 1 mg/mL, and the cells were incubated for another 4 h. The culture medium was carefully removed, and 100 μL of DMSO was added to each well of the plate. The plate was gently shaken to dissolve the purple crystals generated by the MTT reagent. The optical density at 570 nm was recorded on a microplate reader (BioTek Synergy H1 multimode microplate reader).

■ ASSOCIATED CONTENT

Supporting Information

The Supporting Information is available free of charge at https://pubs.acs.org/doi/10.1021/acsami.3c16585.

Synthesis and characterization of BDP derivatives and theranostic prodrugs, UV−vis absorption and fluorescence emission spectra, GSH-sensing titration and selectivity, colloidal stability of nanoprodrugs, drug release profiles, HRMS analysis of released species, the toxicity of BDP derivatives, confocal fluorescence images of BDP derivatives in cancer cells, in vitro antitumor efficacy study in various cancer cells (PDF)

■ AUTHOR INFORMATION

Corresponding Author

Binglin Sui − *Department of Chemistry, University of North Dakota, Grand Forks, North Dakota 58202, United States;* orcid.org/0000-0003-0376-317X; Email: binglin.sui@und.edu

Authors

Safiya Nisar − *Department of Chemistry, University of North Dakota, Grand Forks, North Dakota 58202, United States*

Elisabeth Starosta − *Department of Chemistry, University of North Dakota, Grand Forks, North Dakota 58202, United States*

Mouhmad Elayyan − *Department of Chemistry, University of North Dakota, Grand Forks, North Dakota 58202, United States*

Amrit Regmi − *Department of Chemistry, University of North Dakota, Grand Forks, North Dakota 58202, United States*

Complete contact information is available at: https://pubs.acs.org/10.1021/acsami.3c16585

Notes

The authors declare no competing financial interest.

■ ACKNOWLEDGMENTS

We acknowledge the support from the National Science Foundation (CHE-2213445 and 2117699) and the University of North Dakota Postdoctoral Seed Funding.

■ REFERENCES

(1) Kelkar, S. S.; Reineke, T. M. Theranostics: Combining Imaging and Therapy. *Bioconjugate Chem.* **2011**, *22* (10), 1879−1903.

(2) Rautio, J.; Meanwell, N. A.; Di, L.; Hageman, M. J. The Expanding Role of Prodrugs in Contemporary Drug Design and Development. *Nat. Rev. Drug Discovery* **2018**, *17* (8), 559−587.

(3) Cheetham, A. G.; Chakroun, R. W.; Ma, W.; Cui, H. Self-Assembling Prodrugs. *Chem. Soc. Rev.* **2017**, *46* (21), 6638−6663.

(4) Walther, R.; Rautio, J.; Zelikin, A. N. Prodrugs in Medicinal Chemistry and Enzyme Prodrug Therapies. *Adv. Drug Delivery Rev.* **2017**, *118*, 65−77.

(5) Bildstein, L.; Dubernet, C.; Couvreur, P. Prodrug-Based Intracellular Delivery of Anticancer Agents. *Adv. Drug Delivery Rev.* **2011**, *63* (1), 3−23.

(6) Mahato, R.; Tai, W.; Cheng, K. Prodrugs for Improving Tumor Targetability and Efficiency. *Adv. Drug Delivery Rev.* **2011**, *63* (8), 659−670.

(7) Fang, J.; Nakamura, H.; Maeda, H. The EPR Effect: Unique Features of Tumor Blood Vessels for Drug Delivery, Factors Involved, and Limitations and Augmentation of the Effect. *Adv. Drug Delivery Rev.* **2011**, *63* (3), 136−151.

(8) Maeda, H.; Nakamura, H.; Fang, J. The EPR Effect for Macromolecular Drug Delivery to Solid Tumors: Improvement of Tumor Uptake, Lowering of Systemic Toxicity, and Distinct Tumor Imaging in Vivo. *Adv. Drug Delivery Rev.* **2013**, *65* (1), 71−79.

(9) Min, Y.; Caster, J. M.; Eblan, M. J.; Wang, A. Z. Clinical Translation of Nanomedicine. *Chem. Rev.* **2015**, *115* (19), 11147−11190.

(10) Dadashi-Silab, S.; Doran, S.; Yagci, Y. Photoinduced Electron Transfer Reactions for Macromolecular Syntheses. *Chem. Rev.* **2016**, *116* (17), 10212−10275.

(11) Escudero, D. Revising Intramolecular Photoinduced Electron Transfer (PeT) from First-Principles. *Acc. Chem. Res.* **2016**, *49* (9), 1816−1824.

(12) Lee, Y.-M.; Nam, W.; Fukuzumi, S. Redox Catalysis via Photoinduced Electron Transfer. *Chem. Sci.* **2023**, *14* (16), 4205−4218.

(13) Niu, H.; Liu, J.; O'Connor, H. M.; Gunnlaugsson, T.; James, T. D.; Zhang, H. Photoinduced Electron Transfer (PeT) Based Fluorescent Probes for Cellular Imaging and Disease Therapy. *Chem. Soc. Rev.* **2023**, *52* (7), 2322−2357.
(14) Li, R.; Peng, F.; Cai, J.; Yang, D.; Zhang, P. Redox Dual-Stimuli Responsive Drug Delivery Systems for Improving Tumor-Targeting Ability and Reducing Adverse Side Effects. *Asian J. Pharm. Sci.* **2020**, *15* (3), 311−325.
(15) Phillips, D. J.; Gibson, M. I. Redox-Sensitive Materials for Drug Delivery: Targeting the Correct Intracellular Environment, Tuning Release Rates, and Appropriate Predictive Systems. *Antioxid. Redox Signal.* **2014**, *21* (5), 786−803.
(16) Liu, Y.; Pei, Q.; Chen, L.; Li, Z.; Xie, Z. Reduction-Responsive Fluorescence Off−On BODIPY−Camptothecin Conjugates for Self-Reporting Drug Release. *J. Mater. Chem. B* **2016**, *4* (13), 2332−2337.
(17) Umezawa, K.; Yoshida, M.; Kamiya, M.; Yamasoba, T.; Urano, Y. Rational Design of Reversible Fluorescent Probes for Live-Cell Imaging and Quantification of Fast Glutathione Dynamics. *Nat. Chem.* **2017**, *9* (3), 279−286.
(18) Zheng, Z.; Huyan, Y.; Li, H.; Sun, S.; Xu, Y. A Lysosome-Targetable Near Infrared Fluorescent Probe for Glutathione Sensing and Live-Cell Imaging. *Sens. Actuators, B* **2019**, *301*, No. 127065.
(19) Quinn, J. F.; Whittaker, M. R.; Davis, T. P. Glutathione Responsive Polymers and Their Application in Drug Delivery Systems. *Polym. Chem.* **2017**, *8* (1), 97−126.
(20) Ding, Y.; Dai, Y.; Wu, M.; Li, L. Glutathione-Mediated Nanomedicines for Cancer Diagnosis and Therapy. *Chem. Eng. J.* **2021**, *426*, No. 128880.
(21) Ling, X.; Tu, J.; Wang, J.; Shajii, A.; Kong, N.; Feng, C.; Zhang, Y.; Yu, M.; Xie, T.; Bharwani, Z.; Aljaeid, B. M.; Shi, B.; Tao, W.; Farokhzad, O. C. Glutathione-Responsive Prodrug Nanoparticles for Effective Drug Delivery and Cancer Therapy. *ACS Nano* **2019**, *13* (1), 357−370.
(22) Lu, F.; Sang, R.; Tang, Y.; Xia, H.; Liu, J.; Huang, W.; Fan, Q.; Wang, Q. Fabrication of a Phototheranostic Nanoplatform for Single Laser-Triggered NIR-II Fluorescence Imaging-Guided Photothermal/Chemo/Antiangiogenic Combination Therapy. *Acta Biomater.* **2022**, *151*, 528−536.
(23) Zhang, L.; Zheng, H.; Cui, H.; Yin, X.; Zhang, C.; Wang, Y.; Zhao, Y.; Lin, J.; Wang, Z.; Wang, J.; Chen, Q. Nanomicelle-Based Redox-Responsive Dual-Prodrug for Synergistic Breast Cancer Chemo-Immunotherapy. *ACS Appl. Nano Mater.* **2023**, *6* (19), 18263−18274.
(24) Loudet, A.; Burgess, K. BODIPY Dyes and Their Derivatives: Syntheses and Spectroscopic Properties. *Chem. Rev.* **2007**, *107* (11), 4891−4932.
(25) Ulrich, G.; Ziessel, R.; Harriman, A. The Chemistry of Fluorescent BODIPY Dyes: Versatility Unsurpassed. *Angew. Chem., Int. Ed.* **2008**, *47* (7), 1184−1201.
(26) Kowada, T.; Maeda, H.; Kikuchi, K. BODIPY-Based Probes for the Fluorescence Imaging of Biomolecules in Living Cells. *Chem. Soc. Rev.* **2015**, *44* (14), 4953−4972.
(27) Mao, Z.; Kim, J. H.; Lee, J.; Xiong, H.; Zhang, F.; Kim, J. S. Engineering of BODIPY-Based Theranostics for Cancer Therapy. *Coord. Chem. Rev.* **2023**, *476*, No. 214908.
(28) Zeng, L.; Miller, E. W.; Pralle, A.; Isacoff, E. Y.; Chang, C. J. A Selective Turn-On Fluorescent Sensor for Imaging Copper in Living Cells. *J. Am. Chem. Soc.* **2006**, *128* (1), 10−11.
(29) Wang, L.; Xiao, Y.; Tian, W.; Deng, L. Activatable Rotor for Quantifying Lysosomal Viscosity in Living Cells. *J. Am. Chem. Soc.* **2013**, *135* (8), 2903−2906.
(30) Işık, M.; Guliyev, R.; Kolemen, S.; Altay, Y.; Senturk, B.; Tekinay, T.; Akkaya, E. U. Designing an Intracellular Fluorescent Probe for Glutathione: Two Modulation Sites for Selective Signal Transduction. *Org. Lett.* **2014**, *16* (12), 3260−3263.
(31) Sui, B.; Tang, S.; Liu, T.; Kim, B.; Belfield, K. D. Novel BODIPY-Based Fluorescence Turn-On Sensor for Fe^{3+} and Its Bioimaging Application in Living Cells. *ACS Appl. Mater. Interfaces* **2014**, *6* (21), 18408−18412.
(32) Sui, B.; Yue, X.; Tichy, M. G.; Liu, T.; Belfield, K. D. Improved Synthesis of the Triazacryptand (TAC) and Its Application in the Construction of a Fluorescent TAC-BODIPY Conjugate for K^+ Sensing in Live Cells. *Eur. J. Org. Chem.* **2015**, *2015* (6), 1189−1192.
(33) Sui, B.; Liu, X.; Wang, M.; Belfield, K. D. A Highly Selective Fluorescence Turn-On Sensor for Extracellular Calcium Ion Detection. *Chem. - Eur. J.* **2016**, *22* (30), 10351−10354.
(34) Zhang, J.; Yang, M.; Li, C.; Dorh, N.; Xie, F.; Luo, F.-T.; Tiwari, A.; Liu, H. Near-Infrared Fluorescent Probes Based on Piperazine-Functionalized BODIPY Dyes for Sensitive Detection of Lysosomal pH. *J. Mater. Chem. B* **2015**, *3* (10), 2173−2184.
(35) Zhu, S.; Zhang, J.; Janjanam, J.; Vegesna, G.; Luo, F.-T.; Tiwari, A.; Liu, H. Highly Water-Soluble BODIPY-Based Fluorescent Probes for Sensitive Fluorescent Sensing of Zinc(II). *J. Mater. Chem. B* **2013**, *1* (12), 1722−1728.
(36) Zhang, J.; Yang, M.; Mazi, W.; Adhikari, K.; Fang, M.; Xie, F.; Valenzano, L.; Tiwari, A.; Luo, F.-T.; Liu, H. Unusual Fluorescent Responses of Morpholine-Functionalized Fluorescent Probes to pH via Manipulation of BODIPY's HOMO and LUMO Energy Orbitals for Intracellular pH Detection. *ACS Sens.* **2016**, *1* (2), 158−165.
(37) Sui, B.; Bondar, M. V.; Anderson, D.; Rivera-Jacquez, H. J.; Masunov, A. E.; Belfield, K. D. New Two-Photon Absorbing BODIPY-Based Fluorescent Probe: Linear Photophysics, Stimulated Emission, and Ultrafast Spectroscopy. *J. Phys. Chem. C* **2016**, *120* (26), 14317−14329.
(38) Sui, B.; Tang, S.; Woodward, A. W.; Kim, B.; Belfield, K. D. A BODIPY-Based Water-Soluble Fluorescent Probe for Mitochondria Targeting. *Eur. J. Org. Chem.* **2016**, *2016* (16), 2851−2857.
(39) Sui, B.; Yue, X.; Kim, B.; Belfield, K. D. Near-IR Two-Photon Fluorescent Sensor for K^+ Imaging in Live Cells. *ACS Appl. Mater. Interfaces* **2015**, *7* (32), 17565−17568.
(40) Kuimova, M. K.; Yahioglu, G.; Levitt, J. A.; Suhling, K. Molecular Rotor Measures Viscosity of Live Cells Via Fluorescence Lifetime Imaging. *J. Am. Chem. Soc.* **2008**, *130* (21), 6672−6673.
(41) Oshikawa, Y.; Ojida, A. PeT-Dependent Fluorescence Sensing of Enzyme Reactions Using the Large and Tunable pKa Shift of Aliphatic Amines. *Chem. Commun.* **2013**, *49* (97), 11373−11375.
(42) Ou-Yang, J.; Jiang, W.-L.; Tan, K.-Y.; Liu, H.-W.; Li, S.-J.; Liu, J.; Li, Y.-F.; Li, C.-Y. Two-Photon Fluorescence Probe for Precisely Detecting Endogenous H_2S in Lysosome by Employing a Dual Lock System. *Sens. Actuators, B* **2018**, *260*, 264−273.
(43) Xiao, H.; Zhang, R.; Wu, C.; Li, P.; Zhang, W.; Tang, B. A New pH-Sensitive Fluorescent Probe for Visualization of Endoplasmic Reticulum Acidification During Stress. *Sens. Actuators, B* **2018**, *273*, 1754−1761.
(44) Lee, M. H.; Yang, Z.; Lim, C. W.; Lee, Y. H.; Dongbang, S.; Kang, C.; Kim, J. S. Disulfide-Cleavage-Triggered Chemosensors and Their Biological Applications. *Chem. Rev.* **2013**, *113* (7), 5071−5109.
(45) Guo, X.; Cheng, Y.; Zhao, X.; Luo, Y.; Chen, J.; Yuan, W.-E. Advances in Redox-Responsive Drug Delivery Systems of Tumor Microenvironment. *J. Nanobiotechnol.* **2018**, *16* (1), 74.
(46) Sun, X.; Guo, F.; Ye, Q.; Zhou, J.; Han, J.; Guo, R. Fluorescent Sensing of Glutathione and Related Bio-Applications. *Biosensors* **2023**, *13* (1), 16.
(47) Giustarini, D.; Dalle-Donne, I.; Milzani, A.; Fanti, P.; Rossi, R. Analysis of GSH and GSSG after Derivatization with N-Ethylmaleimide. *Nat. Protoc.* **2013**, *8* (9), 1660−1669.
(48) Liu, Y.-L.; Yu, S.-Y.; An, R.; Miao, Y.; Jiang, D.; Ye, D.; Xu, J.-J.; Zhao, W.-W. A Fast and Reversible Responsive Bionic Transmembrane Nanochannel for Dynamic Single-Cell Quantification of Glutathione. *ACS Nano* **2023**, *17* (17), 17468−17475.
(49) Sun, B.; Luo, C.; Yu, H.; Zhang, X.; Chen, Q.; Yang, W.; Wang, M.; Kan, Q.; Zhang, H.; Wang, Y.; He, Z.; Sun, J. Disulfide Bond-Driven Oxidation- and Reduction-Responsive Prodrug Nanoassemblies for Cancer Therapy. *Nano Lett.* **2018**, *18* (6), 3643−3650.
(50) Hao, D.; Meng, Q.; Jiang, B.; Lu, S.; Xiang, X.; Pei, Q.; Yu, H.; Jing, X.; Xie, Z. Hypoxia-Activated Pegylated Paclitaxel Prodrug Nanoparticles for Potentiated Chemotherapy. *ACS Nano* **2022**, *16* (9), 14693−14702.

https://doi.org/10.1021/acsami.3c16585
ACS Appl. Mater. Interfaces 2024, 16, 6859−6867